Rydberg-State Excitation and Ionization of Argon Atoms Subject to Strong Circularly Polarized Two-Color Few-Cycle Laser Fields

Zhiqiang Wang[1,2], Wei Quan[2,3*], Yanlan Wang[2,3], Xiaolei Hao[1*], Jing Chen[4,5*], and Xiaojun Liu[2,3*]

[1]*Institute of Theoretical Physics and Department of Physics, State Key Laboratory of Quantum Optics and Quantum Optics Devices, Collaborative Innovation Center of Extreme Optics, Shanxi University, Taiyuan 030006, China*
[2]*State Key Laboratory of Magnetic Resonance and Atomic and Molecular Physics, Wuhan Institute of Physics and Mathematics, Innovation Academy for Precision Measurement Science and Technology, Chinese Academy of Sciences, Wuhan 430071, China*
[3]*School of Physical Sciences, University of Chinese Academy of Sciences, Beijing 100049, China*
[4]*Hefei National Research Center for Physical Sciences at the Microscale and School of Physical Sciences, Department of Modern Physics, University of Science and Technology of China, Hefei 230026, China*
[5]*Hefei National Laboratory, Hefei 230088, China*

(Received 22 February 2025; accepted manuscript online 21 March 2025)

The ultrafast excitation dynamics of atoms and molecules exposed to circularly polarized two-color (CPTC) laser fields constitute a fascinating topic in attosecond science. Although extensive research has established the relationship between the Rydberg state excitation (RSE) yields and the CPTC field parameters, such as field amplitude ratios and helicity of two components, the role of the relative phase (ϕ) in modulating RSE efficiency remains unclear. In this work, we theoretically investigate the ϕ dependence of RSE and ionization yields in the co-rotating and counter-rotating circularly polarized two-color (CPTC) few-cycle laser fields by a semiclassical model. We find that, in co-rotating CPTC fields, both RSE and ionization yields display pronounced oscillations as a function of ϕ and these oscillations are significantly suppressed in the counter-rotating configuration, particularly for ionization yields. Moreover, the ratio of RSE to ionization yields exhibits an out-of-phase oscillatory pattern between low- and high-intensity regimes. These results can be comprehended by the unique feature of ϕ dependence of CPTC few-cycle fields, based on our semiclassical analysis. Our results demonstrate that phase-controlled CPTC fields offer a versatile tool for steering ultrafast ionization and RSE dynamics of atoms and molecules.

DOI: 10.1088/0256-307X/42/5/053701 CSTR: 32039.14.0256-307X.42.5.053701

1. Introduction. Advances in the development of laser technology have opened the possibility to observe and manipulate ultrafast electron dynamics in atoms and molecules. When atoms or molecules interact with an intense laser field, the valence electron can be released via tunneling ionization (TI)[1] or multiphoton ionization (MPI).[2,3] After that, the electron wave packets are accelerated by the oscillating laser electric field and part of electron wave packets may return to the ionic core and recollide with it.[4] This process is known as rescattering, which triggers a wealth of fascinating nonlinear physical phenomena, such as high harmonic generation (HHG),[5–7] high-order above-threshold ionization (HATI),[8,9] nonsequential double ionization (NSDI)[10–12] and Rydberg-states excitation (RSE).[13–18]

The ultrafast dynamics of atoms and molecules subject to a circularly polarized two-color (CPTC) laser field are very intriguing[19–21] due to the critical features of the CPTC laser fields. Firstly, the CPTC laser field is highly tunable vie key parameters, including the relative the electric field amplitudes, the relative phase, and polarization helicity. Secondly, in CPTC laser fields, the tunneling and recollision processes could happen in different directions,[22] which is in stark contrast to the case of a linearly polarized laser field, where the field-driven excursion of electrons is mainly confined to one spatial dimension, making it difficult to deconvolve molecular structural information encoded by the tunnel-ionization and rescattering processes.[23–25] Thirdly, the CPTC laser field has significant advantages in generating bright circularly polarized extreme ultraviolet beam[26] and soft-x-ray beam.[27] Finally, the strong-field photoelectron holography has also been extended to the counter-rotating CPTC laser fields.[28,29]

Recently, the CPTC laser fields were used to control the NSDI[30] and Rydberg-state excitation (RSE)[31,32] processes. In these works, it was shown that, in the case of multi-cycle CPTC laser field, the yields of the NSDI and RSE strongly depend on the field amplitude ratios and helicity of two components. Nevertheless, the relative phase (ϕ) effect on the RSE yields has not been mentioned. On the other hand, the relative phase effect of NSDI in CPTC laser fields has been demonstrated in the few-cycle CPTC laser fields[33–35] and, surprisingly, in the CPTC field with

*Corresponding author. Email: charlywing@wipm.ac.cn; xlhao@sxu.edu.cn; chenjing@ustc.edu.cn; xjliu@wipm.ac.cn
© 2025 Chinese Physical Society and IOP Publishing Ltd. All rights, including for text and data mining, AI training, and similar technologies, are reserved.

a pulse duration of 16 cycles.[36] However, the dependence of the RSE process on the relative phase, ϕ, of CPTC few-cycle laser fields, particularly its sensitivity, remains an open question.

In this work, we numerically investigate the ϕ dependence of the yields of RSE and ionization in the co-rotating and counter-rotating CPTC few-cycle laser fields by a semiclassical model. We find that both RSE and ionization yields exhibit oscillations with respect to ϕ in co-rotating CPTC fields, while these oscillations are significantly suppressed in the counter-rotating configuration, particularly for ionization yields. Moreover, the ratio of RSE to ionization yields exhibits an out-of-phase oscillatory pattern between low- and high- intensity regimes. These results can be comprehended by the unique feature of ϕ dependence of CPTC few-cycle fields, based on our semiclassical analysis.

2. Theoretical Method. In this work, we employ a classical-trajectory Monte Carlo (CTMC) model[37–39] to study the ϕ dependence of the RSE and ionization of argon atoms in the co-rotating and counter-rotating circularly polarized two-color (CPTC) few-cycle laser fields. The CPTC laser field consists of two single-color circularly polarized fields with different angular frequencies $\omega_{\rm f}$ and $\omega_{\rm s}$. The combined laser vector potentials in the polarization plane are defined by

$$A_x(t) = \frac{f(t)}{\sqrt{2}}\Big[\frac{E_{\rm f}}{\omega_{\rm f}}\sin(\omega_{\rm f}t) \pm \frac{E_{\rm s}}{\omega_{\rm s}}\sin(\omega_{\rm s}t+\phi)\Big], \quad (1)$$

$$A_z(t) = \frac{f(t)}{\sqrt{2}}\Big[\frac{E_{\rm f}}{\omega_{\rm f}}\cos(\omega_{\rm f}t) + \frac{E_{\rm s}}{\omega_{\rm s}}\cos(\omega_{\rm s}t+\phi)\Big]. \quad (2)$$

Here, the upper sign "+" (the lower sign "−") in the Eq. (1) corresponds to the co-rotating (counter-rotating) CPTC laser fields. $E_{\rm f}$ and $\omega_{\rm f}$ are the amplitude and frequency of the fundamental pulse at 800 nm, $E_{\rm s}$ and $\omega_{\rm s}$ are the amplitude and frequency of the second harmonic at 400 nm. $f(t) = \cos^2(\omega_{\rm f}t/2N)$ is the pulse envelope and N denotes the number of optical cycles for 800 nm. ϕ is the relative phase between the 400 nm and 800 nm ranging from 0 to 2π. The polarization plane lies in xz plane and laser beam propagates along the y axis. The laser pulse contains 2 optical cycles (i.e., $N = 2$). In our simulation, the laser fields $\boldsymbol{E}(t)$ is given by $\boldsymbol{E}(t) = -\partial\boldsymbol{A}(t)/\partial t$. $I_{\rm f}(\propto E_{\rm f}^2)$ and $I_{\rm s}(\propto E_{\rm s}^2)$ denote the laser intensities of the fundamental and second harmonic fields, respectively. Throughout this work, $I_{\rm f}/I_{\rm s} = 10$ and we only mention $I_{\rm f}$ below when the intensity of the CPTC field is discussed.

In the CTMC model, the valence electron is assumed to be released into the continuum by tunneling with a zero initial longitudinal momentum ($p_\parallel$), which is parallel to the instantaneous laser polarization direction, and a Gaussian-like initial transverse momentum ($p_\perp$) perpendicular to the instantaneous laser polarization direction. The initial photoelectron transverse momentum is given randomly in the range of $-1.0\,{\rm a.u.} < p_\perp < 1.0\,{\rm a.u.}$ due to the fact that, for the laser intensities studied in this work, the trajectories with initial transverse momenta beyond this range have negligible weights. The definitions of $p_\perp$ and $p_\parallel$ are given in a rotating coordinate,[16] which rotates along with the circularly polarized laser field. Each electron orbit is weighted by the ADK ionization rate.[40,41]

$$W(t_0, p_\perp) \propto W_0 W_1, \quad (3)$$

$$W_0 = \Big|\frac{(2|I_{\rm p}|)^2}{E(t_0)}\Big|^{2/\sqrt{2|I_{\rm p}|}-1} {\rm e}^{\left[\frac{-2(2|I_{\rm p}|)^{\frac{3}{2}}}{3|E(t_0)|}\right]}, \quad (4)$$

$$W_1 = \frac{\sqrt{2|I_{\rm p}|}}{\pi|E(t_0)|}{\rm e}^{\left[\frac{-p_\perp^2\sqrt{2|I_{\rm p}|}}{|E(t_0)|}\right]}. \quad (5)$$

After tunneling, the motion of this tunnel-ionized electron is determined by the classical Newtonian equation, i.e., $\mathrm{d}^2\boldsymbol{r}/\mathrm{d}t^2 = -\boldsymbol{E}(t) - \nabla V(r)$, where the effective potential $V(r)$ is given by $V(r) = -Z_{\rm eff}/r$, $Z_{\rm eff} = \sqrt{2I_{\rm p}}$ is the effective charge of the ionic core, $I_{\rm p}$ is the ionization potential of the atom in question and r the distance between the tunneled electron and the center of the Coulomb potential. In this adiabatic model, the tunneling exit is given by $r_0 = -I_{\rm p}/E(t_0)$. Note that in the simulation, the Keldysh parameter $\gamma \sim 1$ (omitting the weak $\omega_{\rm s}$ component). This indicates tunneling ionization dominates and we can still approximately use the semiclassical model to describe the electron dynamics.

We examine the energy $E_{\rm final}$ of the electron when the laser pulse ends and focus on the electron trajectories with the energies $E_{\rm final} = \boldsymbol{P}^2/2 - Z_{\rm eff}/r < 0$, where $\boldsymbol{P} = (P_x, P_y, P_z)$ is the final photoelectron momentum. These electrons are captured by the ionic potential, while those with $E_{\rm final} > 0$ stand for the ionized ones. According to our calculations, the photoelectron trajectories recaptured to the ground state have negligible impact on the our results. The weights of the corresponding photoelectron trajectories are summed up to calculate the yields of the RSE and ionization processes, respectively. In our simulation, we sample 4×10^6 points at each relative phase for both co-rotating and counter-rotating CPTC fields. Atomic units (a.u.) are used throughout unless otherwise specified.

3. Results and Discussion. The CTMC calculation results for Ar subject to strong CPTC few-cycle laser fields are presented in Fig. 1. As shown in Fig. 1(a), in co-rotating CPTC laser fields at $I_{\rm f} = 1.5 \times 10^{14}\,{\rm W/cm^2}$, the yields of RSE and ionization oscillate versus the relative phase ϕ. Upon closer scrutiny, it is evident that the phase of the RSE yield oscillation deviates significantly from that of the ionization yields. The minimum and maximum of RSE yields appear at $\phi = 0.6\pi$ and $\phi = 1.4\pi$, respectively. While, the minimum of the ionization yields appears at $\phi = \pi$ and its maximum appears at $\phi = 0$ and $\phi = 2\pi$. A similar result can be identified at a higher laser intensity of $3.0 \times 10^{14}\,{\rm W/cm^2}$, as shown in Fig. 1(b), where the minimum and maximum of the RSE yields shift to $\phi = 0.2\pi$ and $\phi = 1.1\pi$, while the minimum and maximum of the ionization yields remain unchanged.

The ϕ dependence of the ratio between RSE and ionization yields has also been investigated because the ratio is more sensitive to the photoelectron dynamics than the RSE yields. It can be observed that the ratio exhibits a distinct oscillation versus ϕ. At $I_{\rm f} = 1.5 \times 10^{14}\,{\rm W/cm^2}$,

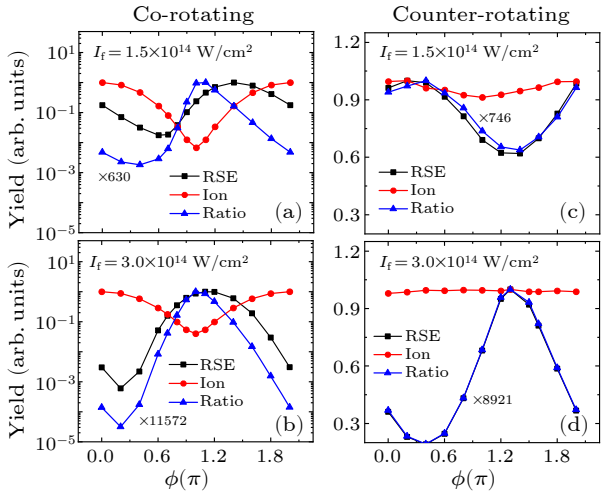

Fig. 1. The calculated relative phase (ϕ) dependence of RSE yields (black squares), ionization yields (red circles) and the ratio of RSE to ionization yields (blue triangles) for co-rotating [(a), (b)] and counter-rotating [(c), (d)] CPTC laser fields at 1.5×10^{14} W/cm^2 [(a), (c)] and 3.0×10^{14} W/cm^2 [(b), (d)], respectively. The calculated data are normalized by the maximum of the corresponding curve. For visual convenience, the curve of ratio is multiplied by a factor, which is indicated in each panel.

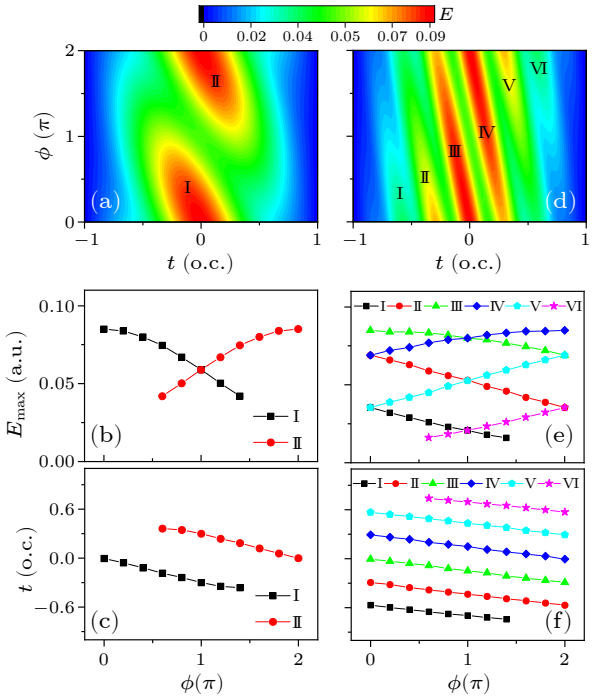

Fig. 2. The strengths of laser electric fields (E) as a function of the relative phase (ϕ) and evolution time (t) in the co-rotating (a) and counter-rotating (d) CPTC laser fields, respectively. The Roman numerals in (a) and (d) represent the peaks that appear in the evolution of the electric field over time. [(b), (c)] and [(e), (f)] derived from (a) and (d), respectively. (b) and (e) indicate the variations of the peak field strength (E_{max}) versus the relative phase (ϕ). (c) and (f) indicate the variations of the instants of E_{max} versus the relative phase. The laser intensity is 3.0×10^{14} W/cm^2.

as shown in Fig. 1(a), the minimum and maximum of the ratio appear at $\phi = 0.4\pi$ and $\phi = 1.1\pi$, respectively. At $I_f = 3.0 \times 10^{14}$ W/cm^2, in Fig. 1(b), the minimum and maximum of the ratio shift to $\phi = 0.2\pi$ and $\phi = \pi$, respectively.

The ϕ dependence of RSE and ionization yields in the counter-rotating CPTC laser fields is presented in Figs. 1(c) and 1(d). In Fig. 1(c), a moderate modulation of the RSE yields and an even weaker modulation of the ionization yields with respect to ϕ can be found. The maximum and the minimum of the ionization yields locate at the relative phases identical to those in the case of co-rotating CPTC fields. The oscillation of the ionization yields is so insignificant that the maximum and minimum of both RSE yields and the ratio appear at $\phi = 0.2\pi$ and $\phi = 1.2\pi$, respectively. Furthermore, at a higher intensity of $I_f = 3.0 \times 10^{14}$ W/cm^2 [Fig. 1(d)], the ionization yields remain almost constant with respect to ϕ. The maximum and minimum of the RSE yields and also the ratio appear at $\phi = 1.3\pi$ and $\phi = 0.4\pi$, respectively. It is interesting to see that the oscillations of RSE (ratio) yields at $I_f = 1.5 \times 10^{14}$ W/cm^2 become almost out of phase with those at $I_f = 3.0 \times 10^{14}$ W/cm^2.

According to our calculations in the laser intensity range explored in this work, the ϕ dependence features will fade or even disappear for longer pulse durations. Specifically, in the counter-rotating CPTC fields, the ϕ dependent RSE oscillations vanish entirely for pulse durations exceeding 3 optical cycles. In contrast, for the co-rotating CPTC fields, the ϕ dependent features persist until the pulse duration surpasses 8 optical cycles.

In order to intuitively comprehend the ϕ dependence of the RSE and ionization yields, we present the strengths of laser electric fields (E) as a function of the relative phase (ϕ) and evolution time (t) in the co-rotating and counter-rotating CPTC laser fields in Figs. 2(a) and 2(d), respectively. As shown in Fig. 2(a), in the co-rotating CPTC laser fields, the strength of the laser electric fields evolves significantly with respect to ϕ and, around $t = 0$, there are two peaks indicated by I and II in Fig. 2(a). At $\phi = 0$, the peak of laser electric field (E_{max}) appears precisely at $t = 0$ and the t distribution of laser electric field is symmetric with respect to $t = 0$. As ϕ increases, the peak I shifts towards the negative direction of the t axis [see black squares in Fig. 2(c)] and its peak field strength gradually weakens [see black squares in Fig. 2(b)]. At $\phi = 1.4\pi$, the strength of peak I becomes so weak that it becomes difficult to determine precisely the apex of peak I. As for the peak II, it will not appear appreciably until $\phi \geq 0.6\pi$. As ϕ increases, E_{max} strength of peak II gradually increases [see red circles in Fig. 2(b)] and the instant corresponding to E_{max} shifts to the negative direction of t axis [see red circles in Fig. 2(c)]. At $\phi = 2\pi$, the field strength of II reaches its maximum and the t distribution of electric field is symmetric with respect to $t = 0$. Note that, although we only present the ϕ and t dependence of laser electric field at 3.0×10^{14} W/cm^2, the evolution law of the laser electric field strength is identical at any laser intensity.

In the case of counter-rotating CPTC laser fields, as shown in Fig. 2(d), the CPTC laser field oscillates more times against t than the case of co-rotating CPTC fields in

the t range presented in this work and the six laser electric field peaks are marked by I–VI. As shown in Fig. 2(e), with increasing ϕ, $E_{\max}$ strength of peaks I–III become gradually weakens, while those of IV–VI become stronger and stronger. Detailed examination reveals that the ϕ dependence of $E_{\max}$ strength is more radical for peaks II and V than the other peaks. Moreover, all six peaks shift towards the negative direction of the t axis as ϕ increases [see Fig. 2(f)]. Generally, the ϕ dependence of both $E_{\max}$ strength and the instant is relatively more moderate in the case of counter-rotating CPTC laser fields, if compared to the case of co-rotating CPTC fields.

To shed more light on the ϕ dependence of ionization yields, we compare the maximum of the electric fields at each ϕ in co-rotating and counter-rotating CPTC laser fields with the ionization yields calculated using the peak field strength $E_{\max}$ and instantaneous laser field $E(t)$, as shown in Fig. 3. As we can see, the ionization yields calculated using both methods exhibit oscillations that are in phase with the peak field strengths of the CPTC fields, although their amplitudes differ. To characterize the relative phase sensitivity of the peak field strengths and the ionization yields, we define a modulation depth parameter, Γ, by $\Gamma = \frac{P_{\max}(\phi)-P_{\min}(\phi)}{P_{\max}(\phi)}$, where $P_{\max}$ ($P_{\min}$) is the maximum (minimum) of ionization yields and $E_{\max}$ strength. As shown in Fig. 3(a), at $1.5\times10^{14}\,\mathrm{W/cm^2}$, in the co-rotating CPTC laser fields, the modulation depths of the peak field strengths and the ionization yields (black squares) are around 32% and 99% at $1.5\times10^{14}\,\mathrm{W/cm^2}$. At a higher intensity of $I_{\mathrm{f}} = 3.0\times10^{14}\,\mathrm{W/cm^2}$ [Fig. 3(b)], the modulation depths of the peak field strengths and the ionization yields remain unchanged, although the curve of ϕ dependence of ionization yields changes slightly. While, in the case of counter-rotating CPTC laser fields at $I_{\mathrm{f}} = 1.5\times10^{14}\,\mathrm{W/cm^2}$, the modulation depths of the peak field strengths and the ionization yields (black squares) are around 5% and 8%, respectively, as shown in Fig. 3(c). At a higher intensity of $I_{\mathrm{f}} = 3.0\times10^{14}\,\mathrm{W/cm^2}$ [Fig. 3(d)],

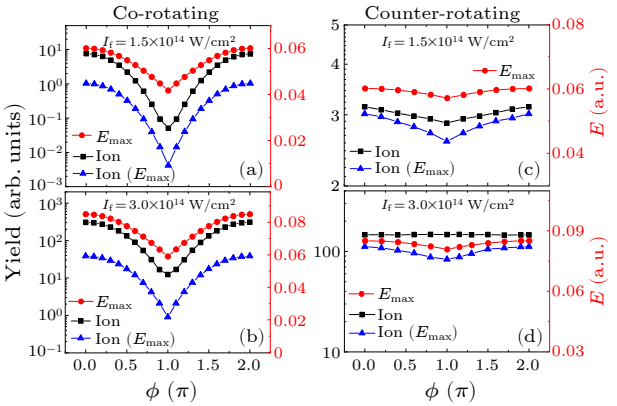

Fig. 3. The calculated ionization yields for Ar subject to the CPTC laser fields by considering a time-dependent laser electric field $E(t)$ [black squares] and an electric field with the strength of $E_{\max}$ [blue triangles], respectively. The ϕ dependence of $E_{\max}$ is also illustrated. The laser fields are co-rotating [(a), (b)] and counter-rotating [(c), (d)] CPTC fields at $1.5\times10^{14}\,\mathrm{W/cm^2}$ [(a), (c)] and $3.0\times10^{14}\,\mathrm{W/cm^2}$ [(b), (d)], respectively. Left axes (black): ionization yields; right axes (red): $E_{\max}$ values.

the modulation depths of the peak field strengths and the ionization yields are around 5% and 1%, respectively. Because that the ionization yields at different relative phases are mainly determined by the corresponding peak field strengths, these results can be well comprehended by the exponential field strength dependence of ADK ionization rate.[40,41] To numerically confirm this, in Fig. 3, we present the ionization yields calculated by the peak strength, i.e., $E_{\max}$, and the results (blue triangles in Fig. 3) faithfully reproduce the results of the time-dependent laser electric field (black squares in Fig. 3).

In the following, we comprehend the ϕ dependence of RSE yields based on the ϕ dependence of the combined laser fields. Generally speaking, there are two main effects which determine the RSE yield. One is the amplitude of the electric field which determines the total yield of the tunneled electron and the final kinetic energy of the electron. The other one is the evolution time defined as the time interval between the tunneling moment and the end of the laser pulse. The latter effect will become important for only few-cycle laser pulses. A similar evolution time effect has been discussed in a recently published paper.[42] As the evolution time increases, electrons propagate further from the ion under laser-induced drift velocity, reducing the Coulomb potential's recapture probability and thereby suppressing the RSE yields. In Figs. 4 and 5, based on the calculations of the CTMC model, we present the t_0 dependence of r (right after the laser pulse ends) distributions of tunneling (including the contributions of both ionization and RSE processes), ionization and RSE yields for $I_{\mathrm{f}} = 1.5\times10^{14}\,\mathrm{W/cm^2}$ and $3\times10^{14}\,\mathrm{W/cm^2}$, respectively, in the co-rotating CPTC laser fields and a series of relative phases (ϕ). In addition, the corresponding laser electric fields and t_0 distributions of the corresponding yields are depicted in these panels. Note that all the distributions are normalized by the corresponding tunneling yields and the lowest row can be applied to demonstrate the ϕ dependence of ratio, instead of the RSE yields.

For the electric field with only one peak [e.g., see Fig. 4(a)], the t_0 dependence of r distribution of tunneling electron shows a triangle structure with one angle extended to large r close to the moment of peak of the field and one angle extended to small r region at later time when the electric field becomes small. This structure can be understood as following: for the co-rotating CPTC laser field, the amplitude of the vector potential changes with the electric field almost synchronously (see Fig. 4), so the electrons tunneled at moment with larger electric field can go to further distance if the evolution time effect is not considered. On the other hand, the width of the initial transverse velocity distribution increases with increasing electric field, hence the width of the r distribution of the electron also increases with increasing amplitude of the field. Therefore, the outline of the r distribution roughly forms an equilateral triangle pattern with the bottom edge parallel to the t_0 axis if the evolution time is not considered. When the evolution time is taken into account, the angle of the triangle at earlier t_0 is lifted up while the angle at later t_0 shifts down to smaller r.

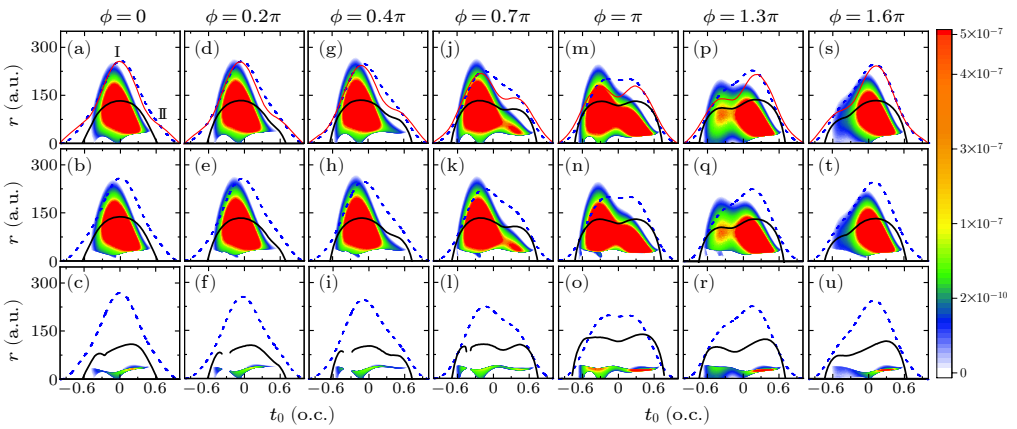

Fig. 4. The r dependence of t_0 distribution of tunneling (a, d, g, j, m, p, s), ionization (b, e, h, k, n, q, t) and RSE (c, f, i, l, o, r, u) processes at the relative phases of $\phi = 0$ [(a)–(c)], $\phi = 0.2\pi$ [(d)–(f)], $\phi = 0.4\pi$ [(g)–(i)], $\phi = 0.7\pi$ [(j)–(l)], $\phi = \pi$ [(m)–(o)], $\phi = 1.3\pi$ [(p)–(r)] and $\phi = 1.6\pi$ [(s)–(u)]. These data are calculated by the CTMC model in the co-rotating CPTC laser fields at 1.5×10^{14} W/cm^2. The blue dashed curves and red solid curves represent the laser vector potential and the laser electric fields at different phases, respectively, and the black solid curves indicate the corresponding t_0 distributions extracted from the 2-dimensional r dependence of t_0 distribution in these panels. Please find more details in the text.

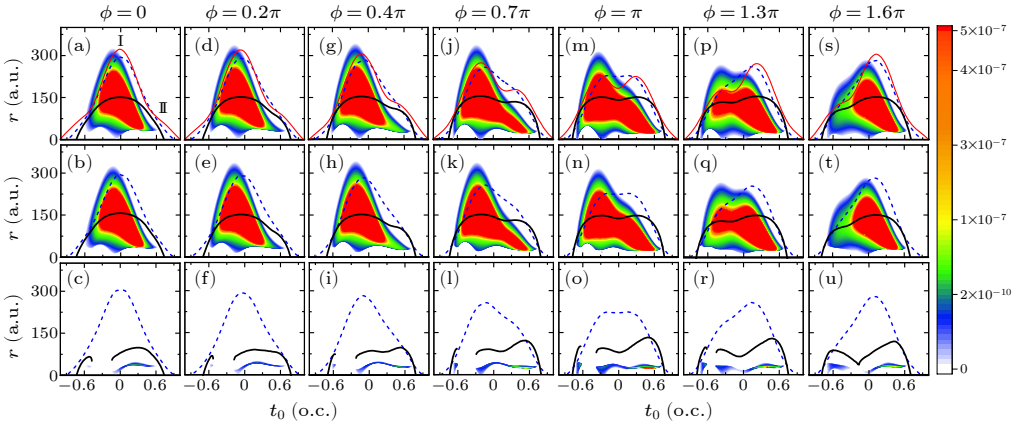

Fig. 5. The r dependence of t_0 distribution of tunneling (a, d, g, j, m, p, s), ionization (b, e, h, k, n, q, t) and RSE (c, f, i, l, o, r, u) processes at the relative phases of $\phi = 0$ [(a)–(c)], $\phi = 0.2\pi$ [(d)–(f)], $\phi = 0.4\pi$ [(g)–(i)], $\phi = 0.7\pi$ [(j)–(l)], $\phi = \pi$ [(m)–(o)], $\phi = 1.3\pi$ [(p)–(r)], and $\phi = 1.6\pi$ [(s)–(u)]. These data are calculated by the CTMC model in the co-rotating CPTC laser fields at 3.0×10^{14} W/cm^2. The blue dashed curves and red solid curves represent the laser vector potential and the laser electric fields at different phases, respectively, and the black solid curves indicate the corresponding t_0 distributions extracted from the 2-dimensional r dependence of t_0 distribution in these panels. Please find more details in the text.

In addition, the upper angle shifts away from the peak of the laser field, making the triangle bias towards negative t_0. Since only the electron with small r and small final kinetic energy can be capture by the ionic Coulomb potential, the RSE yield is largely determined by the shape of the r distribution, especially the position and the probability of the right angle of the triangle structure [see, e.g., Fig. 4(c)], thus the ϕ dependence of the ratio, i.e., the normalized RSE yield, can be understood by analyzing the evolution of the r distribution with varying ϕ.

Let us at first analyze the case of lower intensity. When ϕ increases from 0.2π to 0.4π, the peak of I decreases and shifts to negative time. The r distribution shifts to the left and the probability of small r region is reduced [comparing Fig. 4(d) with Fig. 4(a)], hence the ratio decreases in spite of the increased contribution from the electrons tunneled at around $t_0 = 0.6$ o.c. due to increased electric field [comparing Fig. 4(f) with Fig. 4(c)]. When ϕ increases further, the electric field peak shifts to the left further. However, the significantly reduced vector potential tends to reduce r and eventually leads to down shifted r distribution. In addition, the peak of II, which possesses a much smaller evolution time, becomes more and more important, resulting in fast increasing ratio with increasing ϕ until $\phi = \pi$. At this phase, the electric field is symmetric with respect to the center of the laser pulse with two equal peaks of I and II. More importantly, with significant amplitude, the peak of II possesses almost the latest t_0 and hence the smallest evolution time [see Figs. 2(b) and 2(c)], which leads to pronounced amount of electron in the small r region [see Fig. 4(m)], resulting in the maximal ratio [see Fig. 4(o)]. If the phase ϕ increases further, the amplitude of peak II increases, however, the evolution time increases fast, leading to fast reduced electrons in the small r region [see Fig. 4(p)]. Since the electrons tunneled at the peak II plays a dominant role for the RSE process in this

phase regime, the ratio decreases with increasing ϕ. For the higher intensity of 3×10^{14} W/cm^2, the r distribution varies with ϕ in a similar way as that in the low intensity case. The noticeable difference between two cases is that for higher intensity, the tunneled electron can move significant further at the end of the laser pulse, hence the effect of the evolution time is more important, resulting in more dominant role of the peak Ⅱ as can be seen in Fig. 5. When ϕ increases from 0 to 0.2π, the peak drops and the evolution time increases, so the ratio drops fast. When ϕ increases further, the peak of Ⅱ begins to contribute and surpasses that of the peak of I. Therefore, according to above analysis for the low intensity case, the ratio increases until $\phi = \pi$ and then decreases with increasing ϕ.

In the case of counter-rotating CPTC laser fields, the t_0 dependence of r distributions of tunneling, ionization and RSE normalized yields at 1.5×10^{14} W/cm^2 is depicted in Fig. 6, where the t_0 dependence of E is also presented in each panel. As we can see, the overall r distribution of the tunneled electron shows a shape similar to the co-rotating case [e.g., see Fig. 5(a)], however, since the laser electric field in the counter-rotating CPTC fields oscillates several

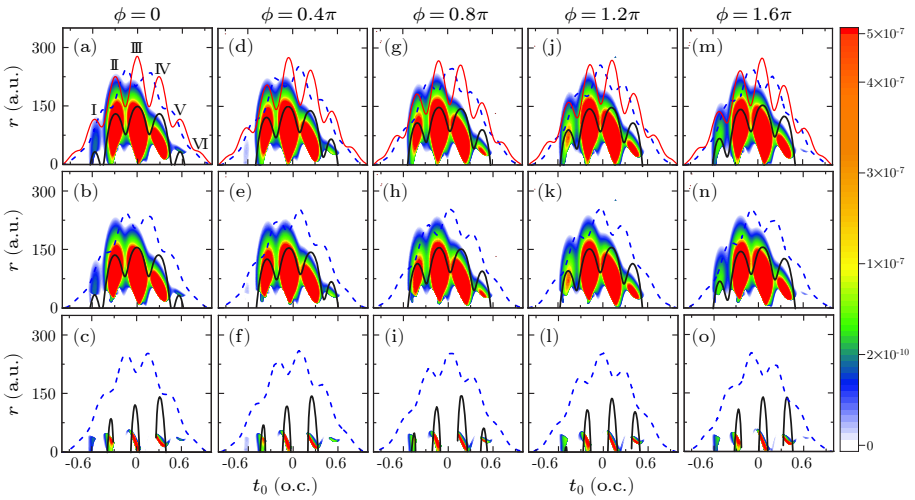

Fig. 6. The r dependence of t_0 distribution of tunneling (a, d, g, j, m), ionization (b, e, h, k, n) and RSE (c, f, i, l, o) processes at the relative phases of $\phi = 0$ [(a)–(c)], $\phi = 0.4\pi$ [(d)–(f)], $\phi = 0.8\pi$ [(g)–(i)], $\phi = 1.2\pi$ [(j)–(l)] and $\phi = 1.6\pi$ [(m)–(o)]. These data are calculated by the CTMC model in the counter-rotating CPTC laser fields at 1.5×10^{14} W/cm^2. The blue dashed curves and red solid curves represent the laser vector potential and the laser electric fields at different phases, respectively, and the black solid curves indicate the corresponding t_0 distributions extracted from the 2-dimensional r dependence of t_0 distribution in these panels. Please find more details in the text.

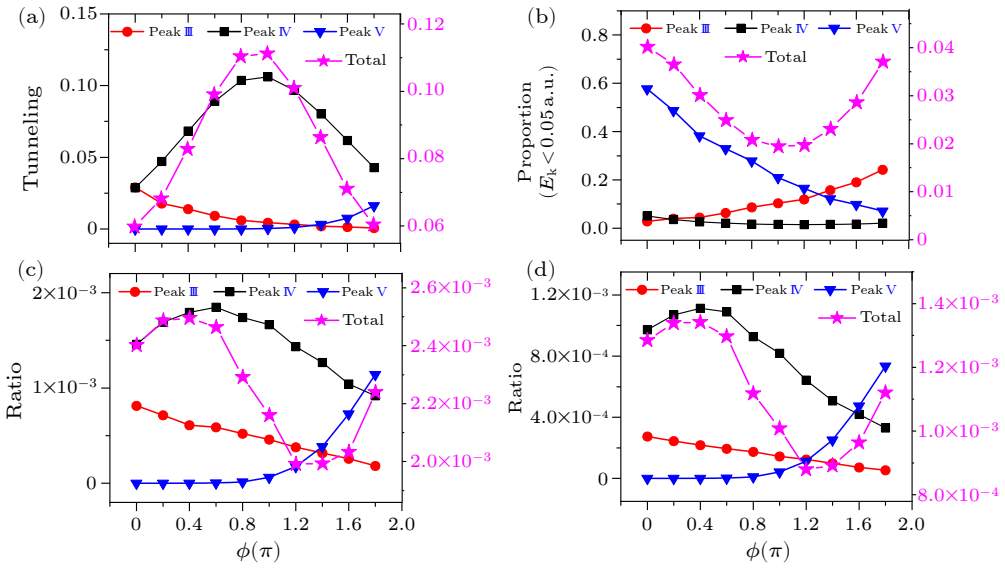

Fig. 7. (a) The phase dependence of tunneling yields for $r < 50$ a.u. (b) The proportion of the electrons with final kinetic energy less than 0.05 a.u. in the data from panel (a) as a function of ϕ. (c) The product of the data from panels (a) and (b) as a function of ϕ. (d) The phase dependence of the ratio. The curves in red, black and blue represent contributions from the peaks Ⅲ, Ⅳ and Ⅴ, respectively. The calculations are performed for the counter-rotating CPTC laser fields at 1.5×10^{14} W/cm^2. Please find more details in the text.

times during the laser pulse [at $\phi = 0$, the laser electric field has six peaks marked by I–VI in Fig. 6(a)], the distribution of the tunneled electrons is divided into several areas. The electrons tunneled from four or five peaks (from I–V) appear in the distribution of tunneling, nevertheless, only four of them (peak Ⅱ to V) contribute to the RSE yield significantly when ϕ varies (see Fig. 6). In Fig. 7(a), we plot the phase dependence of the probability of the tunneled electron with r less than 50 a.u. This probability increases with ϕ until $\phi = \pi$ and then decreases with increasing ϕ, in contrast to the RSE yield which peaks at $\phi = 0.2\pi$ but reaches minimum at $\phi = 1.2\pi$. This result is different from the co-rotating case where the phase dependence of the probability of small r region is qualitatively in agreement with that of the RSE yield (not shown here). It is worth noting that, beside the small distance r which indicates strong Coulomb potential at the end of the laser pulse, the final kinetic energy of the electron is also important in determination of the capture probability of the electron. So in Fig. 7(b) we plot the phase dependent proportion of the electron with final kinetic energy less than 0.05 a.u. for the electrons depicted in Fig. 7(a). One can see that the proportion decreases fast at first, reaches minimum at $\phi = 1.2\pi$ and then increases with ϕ. When the effect of kinetic energy is considered, the probability, as can be considered as the product of two curves depicted in Figs. 7(a) and 7(b) [see Fig. 7(c)], is in good agreement with the RSE yield shown in Fig. 1(c).

To further explore the influence of the field on the RSE yield, we show the probability of small r region and proportion of small kinetic energy for electrons tunneled at peaks of Ⅲ to V, which contribute to the RSE significantly, in Fig. 7 as well. For peak Ⅲ, its contribution to electron with small r drops continuously with ϕ since its amplitude is maximal at $\phi = 0$ and decreases and shifts to negative t_0 with increasing ϕ [see Fig. 7(a)]. Though the proportion of electrons with small kinetic energy of this peak increases with ϕ due to decreasing vector potential [see Fig. 7(b)], the contribution to the RSE yield still drops [see Figs. 7(c) and 7(d)]. For peak Ⅳ, its contribution in the small r region is about the same as that of peak Ⅲ at $\phi = 0$ since, though its amplitude is lower than that of peak Ⅲ, its evolution time is shorter than peak Ⅲ.

When ϕ increases, the amplitude of peak Ⅳ increases and the r distribution expands [e.g., comparing Fig. 6(g) with Fig. 6(d)], leading to increasing probability in the small r region until $\phi = \pi$. When ϕ increases further, the evolution time effect becomes strong, so the probability in the small r region decreases. On the other hand, the proportion of the electrons with small kinetic energy continuously drops due to increasing vector potential with increasing ϕ. As a result, the contribution of peak Ⅳ to the RSE yield increases at first but starts to drop earlier at about $\phi = 0.6\pi$ as can be seen in Figs. 7(c) and 7(d). For peak V, its r distribution evolves in the range where the amplitude of the peak plays a dominant role, so its probability in the small r region increases from a negligible value to a value comparable to that of peak Ⅳ. Considering that its vector potential keeps smaller than that of peak Ⅳ in the whole phase range, its proportion of electrons with small kinetic energy is always larger than that of peak Ⅳ, hence its contribution to the RSE yield keeps rising with increasing ϕ and eventually exceeds that of peak Ⅳ. Therefore, the overall probability of small r region of the tunneled electron largely follows the shape of that of peak Ⅳ while the overall proportion of electrons with small kinetic energy decreases until $\phi = 1.2\pi$ and then increases with ϕ. As a result, the ratio, i.e., the normalized RSE yield reaches a maximum at about $\phi = 0.2\pi - 0.4\pi$ and minimum at $\phi = 1.2\pi$.

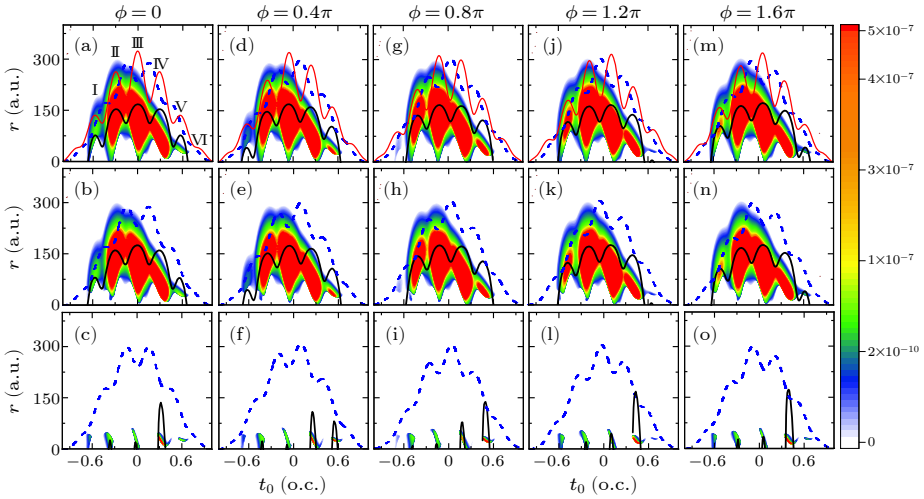

Fig. 8. The r dependence of t_0 distribution of tunneling (a, d, g, j, m), ionization (b, e, h, k, n) and RSE (c, f, i, l, o) processes at the relative phases of $\phi = 0$ [(a)–(c)], $\phi = 0.4\pi$ [(d)–(f)], $\phi = 0.8\pi$ [(g)–(i)], $\phi = 1.3\pi$ [(j)–(l)] and $\phi = 1.6\pi$ [(m)–(o)]. These data are calculated by the CTMC model in the counter-rotating CPTC laser fields at 3.0×10^{14} W/cm^2. The blue dashed curves and red solid curves represent the laser vector potential and the laser electric fields at different phases, respectively, and the black solid curves indicate the corresponding t_0 distributions extracted from the 2-dimensional r dependence of t_0 distribution in these panels. Please find more details in the text.

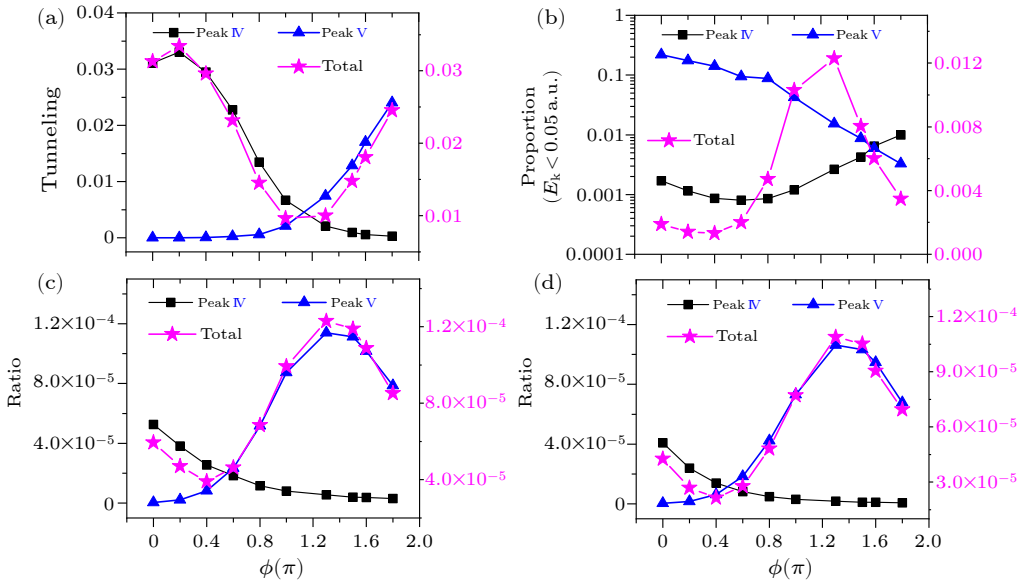

Fig. 9. (a) The phase dependence of tunneling yields for $r < 50$ a.u. (b) The proportion of the electrons with final kinetic energy less than 0.05 a.u. in the data from panel (a) as a function of ϕ. (c) The product of the data from panels (a) and (b) as a function of ϕ. (d) The phase dependence of the ratio. The curves in black and blue represent contributions from the peaks Ⅳ and Ⅴ, respectively. The calculations are performed for the counter-rotating CPTC laser fields at 3.0×10^{14} W/cm^2. Please find more details in the text.

For counter-rotating case with laser intensity of 3×10^{14} W/cm^2, the corresponding typical distributions are depicted in Fig. 8. Similar to the co-rotating case, the electrons tunneled from later peaks, i.e., peaks Ⅳ and Ⅴ, dominates the RSE yield at this higher intensity due to much stronger evolution time effect. For peaks Ⅳ and Ⅴ, we show the same analysis as the low intensity case in Fig. 9. It can be seen that, due to dominating effect of evolution time on peak Ⅳ and effect of peak amplitude on peak Ⅴ, the probability of small r region decreases for peak Ⅳ but increases for peak Ⅴ with increasing ϕ. For the kinetic energy effect, the proportion for peak Ⅳ decreases with ϕ at first but starts to increase when ϕ exceeds 0.4π [see Fig. 9(b)]. This can be understood considering that when the electric field is too high and the evolution time is large, only electrons with small kinetic energy can be close to the core after the end of the pulse. For the peak Ⅴ, the amplitude of the field is not so high and the evolution time is relatively short, so the proportion of electrons with small kinetic energy decreases with increasing ϕ, i.e., increasing vector potential. As a result, the overall proportion follows the curve of peak Ⅳ at first, then rises due to considerable contribution from peak Ⅴ and drops down when peak Ⅴ become dominant. Therefore, the ratio drops, following the curve of peak Ⅳ, and increases until $\phi = 1.3\pi$ and then decreases, closely following the curve of peak Ⅴ, as can be seen in Figs. 9(c) and 9(d). It is worthwhile mentioning that though the proportion of electrons with small kinetic energy also changes with ϕ, they do not modify the ratio qualitatively in the co-rotating cases according to our calculation (not shown here).

Conclusion. In conclusion, we theoretically investigate the ϕ dependence of Rydberg-state excitation (RSE) and ionization in the co-rotating and counter-rotating circularly polarized two-color (CPTC) few-cycle laser fields by a semiclassical model. We find that the yields of both RSE and ionization are highly sensitive to ϕ in co-rotating CPTC fields. On the other hand, in the case of counter-rotating CPTC fields, the RSE yields are still sensitive to ϕ, while the ionization yields become relatively insensitive to ϕ, especially in the high-intensity regime. Moreover, an out-of-phase oscillation with respect to ϕ has been identified for the ratio between the RSE and ionization yields in the low- and high-intensity regimes. These results have been well comprehended by the ϕ dependent multiple-peak structure of the electric fields of CPTC fields and the contributions from these peaks to the RSE yield and their dependence on ϕ strongly depends on the laser intensity, based on a semiclassical analysis.

Acknowledgements. This work is supported by the National Natural Science Foundation of China (Nos. 12121004, 12274273, and 12450402), the Science and Technology Department of Hubei Province (No. 2020CFA029), CAS Project for Young Scientists in Basic Research (No. YSBR-091), and the Youth Innovation Promotion Association CAS (No. 2021328).

References

[1] Milošević D B and Ehlotzky F 2003 *Adv. At. Mol. Opt. Phys.* **49** 373
[2] Agostini P, Fabre F, Mainfray G, Petite G, and Rahman N K 1979 *Phys. Rev. Lett.* **42** 1127
[3] Hansch P, Walker M A, and van Woerkom L D 1998 *Phys. Rev. A* **57** R709
[4] Corkum P B 1993 *Phys. Rev. Lett.* **71** 1994
[5] Ferray M, L'Huillier A, Li X F, Lompre L A, Mainfray G, and Manus C 1988 *J. Phys. B* **21** L31

[6] Gao X Z, Landsman A S, Cao H, Zhang Y, Wang Y, Fu Y, and Pi L W 2022 *Phys. Rev. A* **106** 053105
[7] Shiner A D, Schmidt B E, Trallero-Herrero C, Wörner H J, and Patchkovskii S 2011 *Nat. Phys.* **7** 464
[8] Paulus G G, Nicklich W, Xu H, Lambropoulos P, and Walther H 1994 *Phys. Rev. Lett.* **72** 2851
[9] Wang Y L, Yu S G, Lai X Y, Liu X J, and Chen J 2017 *Phys. Rev. A* **95** 063406
[10] Becker W, Liu X J, Ho P J, and Eberly J H 2012 *Rev. Mod. Phys.* **84** 1011
[11] Walker B, Sheehy B, DiMauro L F, Agostini P, Schafer K J, and Kulander K C 1994 *Phys. Rev. Lett.* **73** 1227
[12] de Morisson Faria C F and Liu X 2011 *J. Mod. Opt.* **58** 1076
[13] Xu S P, Liu M Q, Hu S L, Shu Z, Quan W, Xiao Z L, Zhou Y, Wei M Z, Zhao M, Sun R P, Wang Y L, Hua L Q, Gong C, Lai X Y, Chen J, and Liu X J 2020 *Phys. Rev. A* **102** 043104
[14] Xu S P, Liu M Q, Quan W, Yi X P, Hu S L, Zheng L B, Wang Z Q, Zhao M, Yu S G, Sun R P, Wang Y L, Hua L Q, Lai X Y, Becker W, Chen J, and Liu X J 2022 *Phys. Rev. A* **106** 063106
[15] Wang Z, Quan W, Hao X, Chen J, and Liu X 2023 *Front. Phys.* **11** 1120654
[16] Wang Z Q, Quan W, Hao X L, Chen J, and Liu X J 2024 *Phys. Rev. A* **110** 013114
[17] Liu Y N, Xu S P, Zhu M F, Xiao Z R, Yu S G, Hua L Q, Lai X Y, Quan W, Yang W X, and Liu X J 2023 *Chin. Phys. Lett.* **40** 103201
[18] Zhao J, Liu J, Wang X, and Zhao Z 2024 *Chin. Phys. Lett.* **41** 013201
[19] Mancuso C A, Hickstein D D, Dorney K M, Ellis J L, Hasović E, Knut R, Grychtol P, Gentry C, Gopalakrishnan M, Zusin D, Dollar F J, Tong X M, Milošević D B, Becker W, Kapteyn H C, and Murnane M M 2016 *Phys. Rev. A* **93** 053406
[20] Zhang H D, Guo J, Shi Y, Du H, Liu H F, Huang X R, Liu X S, and Jing J 2017 *Chin. Phys. Lett.* **34** 014206
[21] Qiao Y, Chen J, Zhou S, Chen J, Jiang S, and Yang Y 2024 *Chin. Phys. Lett.* **41** 014205
[22] Fleischer A, Kfir O, Diskin T, Sidorenko P and Cohen O 2014 *Nat. Photonics* **8** 543
[23] Küpper J 2014 *Nat. Phys* **10** 550
[24] Meckel M, Staudte A, Patchkovskii S, Villeneuve D M, Corkum P B, Dörner R and Spanner M 2014 *Nat. Phys.* **10** 594
[25] Shafir D, Mairesse Y, Villeneuve D M, Corkum P B, and Dudovich N 2009 *Nat. Phys.* **5** 412
[26] Kfir O, Grychtol P, Turgut E, Knut R, Zusin D, Popmintchev D, Popmintchev T, Popmintchev H, Shaw J M, Shaw A, Kapteyn H, Murnane M, and Cohen O 2015 *Nat. Photon* **9** 99
[27] Fan T, Grychtol P, Knut R, Hickstein D D, Zusin D, Gentry C, Dollar F *et al.* 2015 *Proc. Natl Acad. Sci. USA* **112** 14206
[28] Li M, Jiang W C, Xie H, Luo S, Zhou Y, and Lu P 2018 *Phys. Rev. A* **97** 023415
[29] Ke Q, Zhou Y, Tan J, He M, Liang J, Zhao Y, Li M, and Lu P 2019 *Opt. Express* **27** 032193
[30] Chaloupka J L and Hickstein D D 2016 *Phys. Rev. Lett.* **116** 143005
[31] Cao C, Li M, Liang J, Guo K, Zhou Y, and Lu P 2021 *J. Phys. B* **54** 035601
[32] Zhang W, Ma Y, Lu C, Chen F, Pan S, Lu P, Ni H, and Wu J 2023 *Adv. Photonics* **5** 016002
[33] Xu T T, Zhang L L, Jin Z, and Gong W J 2020 *Chin. Phys. B* **29** 093202
[34] Huang C, Pang H L, Huang X F, Zhong M M, and Wu Z M 2020 *Opt. Express* **28** 10505
[35] Li Y, Zhang K, Qin L, Chen H, Kang S, Li Z, Wu Y, Xu J, Zhai C, Tang Q, and Yu B 2023 *Optics commum.* **546** 129794
[36] Peng M, Bai L H, and Guo Z 2021 *Commun. Theor. Phys* **73** 075501
[37] Nubbemeyer T, Gorling K, Saenz A, Eichmann U, and Sandner W 2008 *Phys. Rev. Lett.* **101** 233001
[38] Ge P and Liu Y 2017 *J. Phys. B* **50** 125001
[39] Chen J, Liu J, Fu L B, and Zheng W M 2000 *Phys. Rev. A* **63** 011404
[40] Ammosov M V, Delone N B, and Delone V P 1986 *Sov. Phys. JETP* **64** 1191
[41] Perelomov A M, Popov V S, and Terent'ev M V 1966 *Sov. Phys. JETP* **23** 924
[42] Zhao L Y, Liu J L, Jiang T, Lang Y, and Zhao Z X 2024 *Acta Phys. Sin.* **73** 243201 (in Chinese)